CILAMCE 2017
Florianópolis - Santa Catarina - Brazil

VORTEX SHEDDING BY LES 3D NUMERICAL SIMULATION

Marcela L. Santos

marcela.lsantos@coc.ufrj.br

Programa de Engenharia Civil – COPPE/UFRJ / Instituto Multidisciplinar – UFRRJ

Av. Horácio Macedo 2030, Cidade Universitária, 21941-972, Rio de Janeiro, Brasil / Av. Governador Roberto Silveira S/N, Centro, 26020740, Nova Iguaçu, Rio de Janeiro, Brasil

Michèle S. Pfeil

Alvaro L. G. A. Coutinho

mpfeil@coc.ufrj.br

alvaro@nacad.ufrj.br

Programa de Engenharia Civil – COPPE/UFRJ

Av. Horácio Macedo 2030, Cidade Universitária, 21941-972, Rio de Janeiro, Brasil

Abstract. *Slender tower and chimney structures usually have uniform or tapered circular cross-sections and may display significant wind induced vibrations due to vortex shedding. It is of fundamental importance to understand how the flow develops around the structure. In this perspective, the present study focuses on the numerical simulation of the flow around fixed rigid tower structures for which experimental results from wind tunnel tests are available in the literature, for both uniform and shear wind velocity profiles at low Reynolds numbers. The solution of the incompressible Navier-Stokes equations is obtained by 3D Computational Fluid Dynamics (CFD), considering Smagorinsky's LES turbulence model. The main goal of the analyses is to validate the numerical models, to allow future numerical studies on the influence of turbulence on the behavior of towers and chimneys under wind action. The results are very satisfactory, ensuring the adequacy of the developed models.*

Keywords: *Computational fluid dynamics, Vortex shedding, Uniform and tapered cylinder, 3D numerical simulation*

1 INTRODUCTION

Towers and chimneys under wind flow are submitted to fluctuating lateral forces due to vortex-shedding and may display large amplitude vibration when fluid-structure mechanisms are developed, the so-called vortex-induced vibrations. For these structures that are usually constant-diameter or tapered circular cross section bodies under turbulent wind flow the physics of the near wake becomes very complex due to many sources of three-dimensionalities and high Reynolds number flow regime.

Usually, research related to wind action in structures are developed by measuring in situ or reduced-scale wind-tunnel testing. The numerical simulation by Computational Fluid Dynamics (CFD) is another alternative for flow analysis, aiming to solve the Navier-Stokes equations. The applicability of CFD techniques is mainly associated with the need to represent complex models that have large operational request or large scales of representation that is impractical to be developed in the laboratory. Also, whether compared with reduced-scale experiments, CFD simulation makes it easy the study of problems when is considered changing model's configuration, as well as the measurements in difficult access location points.

Figure 1 shows the relationship between Reynolds number and Strouhal number, obtained from experimental models of circular cylinders in two-dimensions flow conditions. Considering towers and chimneys geometric characteristics and wind velocities the corresponding Reynolds number range is 3.0×10^5 to 3×10^7.

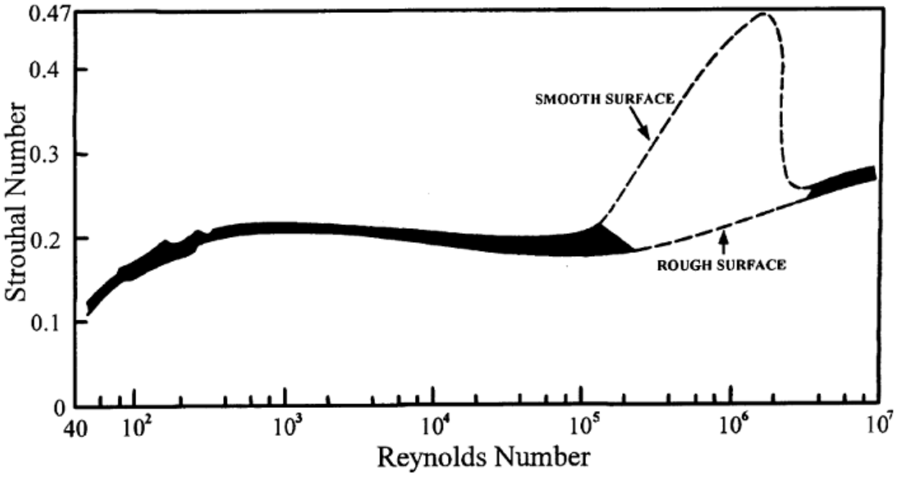

Figure 1. The Strouhal-Reynolds number relation (Blevins, 1977)

One important feature of the flow behind a circular cylinder is the variation of the vortex-shedding frequency in the wake along the cylinder span. Fig. 2 (Hsiao and Chiang, 1998) show experimental results obtained for constant diameter and tapered cylinders under uniform inflow at Reynolds number range $1 - 1.4 \times 10^4$. Narrow bandwidth autospectra of cross wind velocities can be noted in Fig. 2a related to the uniform circular cylinder indicating that well-defined streamwise vortices of constant frequency are shed along the cylinder axis. For the tapered structure, the vortex shedding frequency varies in steps giving rise to regions of constant frequency called vortex cells. The vortex cells formation first observed about tapered cylinders at low Re, from 30 to 300 (König et al., 1992, Williamson, 1989), outside practical engineering situations, but has been confirmed to exist for higher Re values as well. This behavior may also

Proceedings of the XXXVIII Iberian Latin-American Congress on Computational Methods in Engineering
P.O. Faria, R.H. Lopez, L.F.F. Miguel, W.J.S. Gomes, M. Noronha (Editores), ABMEC, Florianópolis, SC, Brazil, November 5-8, 2017.

be triggered by shear (or non-uniform) inflow for constant-diameter cylinders or other three-dimensionality sources such as end effects or diameter discontinuity.

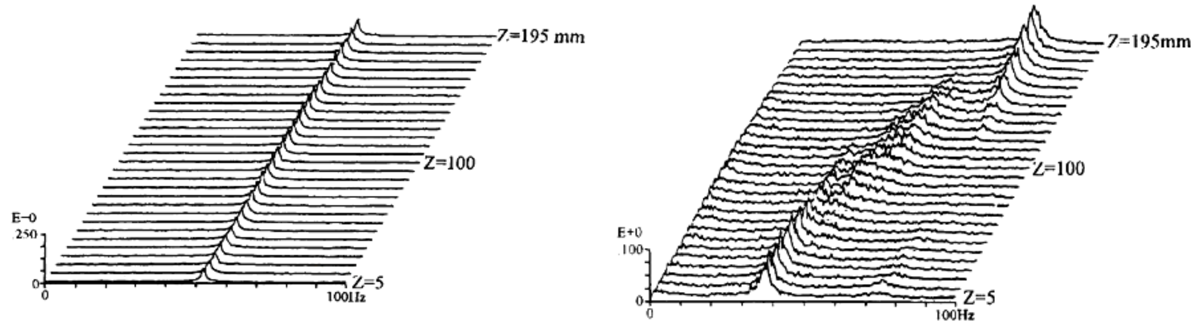

(a) (b)

Figure 2. Autospectrum: (a) uniform cylinder; (b) tapered cylinder. (Hsiao & Chiang, 1998)

The influence of Reynolds number Re and taper ratio on the vortex shedding frequency as well as the characteristics of the intersection region in between two neighboring vortex cells were investigated by Hsiao and Chiang (1998) among others. They found that the transition from one cell to another can be abrupt (for lower values of Re) or smooth (for higher Re). In the last case, they also observed longer interception regions. A useful graphic form of the flow in these regions is the pseudo-flow visualization. By acquiring time histories of the cross-flow velocity at one arbitrary point in the wake along spanwise direction of the cylinder, contour lines of velocity may be depicted as shown in Fig. 3. If the vortex lines are aligned through the span then the shedding frequency is constant as opposed to the cellular behavior in which stepwise varying frequency is observed. The non-alignment of the vortices between adjacent cells is known as "vortex dislocations" or "vortex splits".

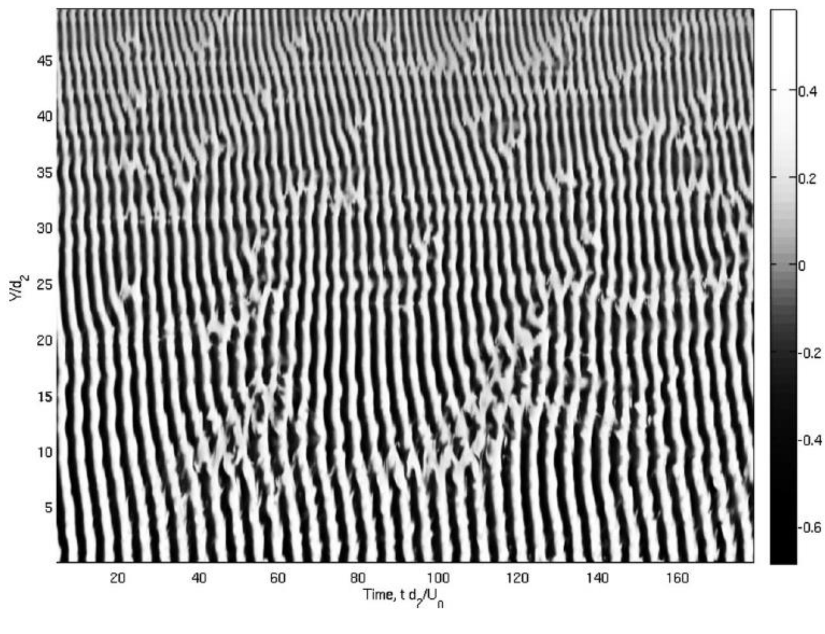

Figure 3. Contour lines of velocity. (Narsimhamurthy *et al.*, 2009)

According to Bargi *et al.* (2015) most 3D numerical simulation of vortex shedding past cylinders or of vortex-induced oscillation deal with the constant-diameter case. Vortex shedding behind stationary tapered cylinders was addressed by many of authors (e.g., Narsimhamurthy *et al.*, 2009) and also the case of elastically mounted cylinders to investigate vortex-induced response (Bargi *et al.*, 2015), all considering uniform inflow conditions.

The present research work aims to perform 3D numerical simulation of tapered towers under turbulent wind action for the stationary or vibrating structure. As a first step, validation of numerical models is presented here to ensure the adequacy of the models. The solution of the incompressible Navier-Stokes equations is obtained by 3D Computational Fluid Dynamics (CFD) considering Smagorinsky´s LES turbulence model. An example of stationary tapered structures under uniform inflow velocity is considered with the following characteristics: taper ratio $= 75$; $102 < Re < 300$ (Narsimhamurthy *et al.*, 2009). The remainder of this paper is organized as follows. Section 2 presents the computational approach. In Section 3 we discuss the examples and numerical models. Section 4 discusses the results and the paper ends with a summary of our main findings.

2 COMPUTATIONAL APPROACH

For Newtonian fluids, the equations governing incompressible fluid flow are the continuity equation (conservation of mass) and Navier-Stokes equations (conservation of momentum). Consider a spatial fluid domain $\Omega_t \in \mathbb{R}^3$, boundary Γ_t and time t, these equations can be described respectively as:

$$\nabla \cdot \boldsymbol{u} = \boldsymbol{0}, \tag{4}$$

$$\rho\left(\frac{\partial \boldsymbol{u}}{\partial t} + \boldsymbol{u} \cdot \nabla \boldsymbol{u} - \boldsymbol{f}\right) - \nabla \cdot \boldsymbol{\sigma} = \boldsymbol{0}, \tag{5}$$

where $\boldsymbol{u}$ is the velocity vector, p is the pressures, $\boldsymbol{f}$ is the external forces and $\boldsymbol{\sigma}$ is the stress tensor defined as:

$$\boldsymbol{\sigma}(\boldsymbol{u}, p) = -p\boldsymbol{I} + 2\mu\boldsymbol{\varepsilon}(\boldsymbol{u}), \tag{6}$$

where $\boldsymbol{I}$ is the unit tensor, the term $2\mu\boldsymbol{\varepsilon}(\boldsymbol{u})$ represents the viscous stress tensor, for which μ is the dynamic viscosity and $\boldsymbol{\varepsilon}(\boldsymbol{u})$ is the strain rate tensor:

$$\boldsymbol{\varepsilon}(\boldsymbol{u}) = \frac{1}{2}(\boldsymbol{\nabla}\boldsymbol{u} + (\boldsymbol{\nabla}\boldsymbol{u})^{\mathrm{T}}), \tag{7}$$

The boundary conditions, which define the problem in incompressible flow, are the Dirichlet and Neumann conditions. The initial conditions are:

$$\boldsymbol{u}(\boldsymbol{x}, 0) = \boldsymbol{u}_0. \tag{8}$$

In practice, most flows developed are turbulent, three-dimensional and time dependent. Consequently, a important feature of turbulent flows is the multiplicity of scales. The large eddy structures have low frequency, being controlled by the geometry, and the smaller eddy have high frequency and are controlled by the fluid viscosity.

The Navier-Stokes equations allow to verify the behavior of different types of flows, turbulent or not. The Direct Numerical Simulation (DNS) consider numerical solving the Navier-Stokes equations for all the motions in a turbulent flow. However, the computational cost is very high, due to the limitation of the processing speed and the memory of the computer. This is consequence to the high number of operations required, since the fact that the number of grid points (N) needed is $N^3 > Re^{9/4}$, in order to ensure that all of the important structures of the turbulence have been captured (Ferziger & Peric, 2002).

The Large Eddy Simulation (LES) is based on the observation that the small turbulent structures are homogeneous and isotropic, more universal than the large scales which carry the turbulent energy. Therefore, the main objective of this method is to solve the large scales structures, by direct solution of the Navier-Stokes equations, approaching the effects of the small scales by mathematical models.

The DNS and LES methods have a significant similarity, since both depend the direct solution of the Navier-Stokes equations, conserving the three-dimensionality and transient conditions of the flow formulation. A consequence of this similarity is the requirement of refined meshes. However, the LES can simulate high numbers of Reynolds flows, using a filtering process between scales, that allows to identify in the grid the smaller scale. The eddies below this scale will be reproduced by subgrid models, while the DNS method capture only the smallest scales whether the mesh has a larger discretization (Fig. 4).

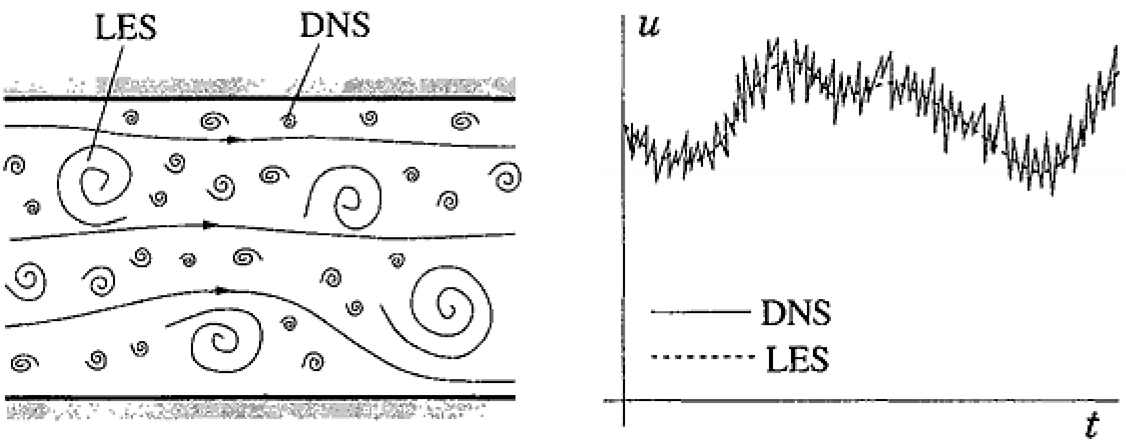

(a) (b)

Figure 4. Schematic relationship between DNS and LES methods (a) representation of turbulent motion; (b) the time dependence of a velocity component at a point. (Ferziger & Peric, 2002).

The LES simulation is based on a spatial filtering operation, so that it is necessary to decompose the flow variables into large scale components, $\bar{f}(\boldsymbol{x},t)$, and into a small scales (subgrid), $f'(\boldsymbol{x},t)$.

$$f(\boldsymbol{x},t) = \bar{f}(\boldsymbol{x},t) + f'(\boldsymbol{x},t). \tag{9}$$

So, the filtered variable is expressed as:

$$\bar{f}(\boldsymbol{x},t) = \int_D f'(\boldsymbol{x}',t)G(\boldsymbol{x}-\boldsymbol{x}')d\boldsymbol{x}, \tag{10}$$

where G is the filter function, determining the structure and size of the small scales. The filter function depends on the difference $(\boldsymbol{x}-\boldsymbol{x}')$ and the width of the filter Δ. The mostly used filter functions are the Gaussian, Fourier cut-off and real space filter. The last filter is defined by:

$$G(\boldsymbol{x}) = \begin{cases} 1/\Delta^3 & se\ |x| \le \Delta/2 \\ 0 & se\ |x| > \Delta/2 \end{cases}. \tag{11}$$

When the Navier-Stokes equations with constant density (for incompressible flow), Eq. 5, and conservation of mass, Eq. 4, are filtered, the governing equations can be written as

$$\frac{\partial \overline{u_i}}{\partial x_i} = 0, \tag{12}$$

$$\rho \frac{\partial \overline{u_i}}{\partial t} + \rho \frac{\partial \overline{u_i u_j}}{\partial x_j} = \rho f_i - \frac{\partial \overline{p}}{\partial x_i} + \mu \frac{\partial^2 \overline{u_i}}{\partial x_j^2}. \tag{13}$$

Because the continuity equation is linear, filtering does not change, and Eq. 4 is formally similar to Eq. 12.

In Eq. 13, however, it shoud be noted the presence of a non-linear convective term on the form of the filtered product $\overline{u_\iota u_J}$, so it is impossible to solve Eq. (13), since the filtered product is not commutative.

To eliminate this problem, the combination $\overline{u}_\iota \overline{u}_J$ is considered, resulting in a new equation:

$$\rho \frac{\partial \overline{u_i}}{\partial t} + \rho \frac{\partial \overline{u_i u_j}}{\partial x_j} = \rho f_i - \frac{\partial \overline{p}}{\partial x_i} + \mu \frac{\partial^2 \overline{u_i}}{\partial x_j^2} - \frac{\partial \tau_{ji}}{\partial x_j}, \tag{14}$$

where τ_{ji} is the terms of the subgrid scale Reynolds-stress tensor:

$$\tau_{ji} = \overline{u_\iota u_J} - \overline{u}_\iota \overline{u}_J. \tag{15}$$

The tensor τ_{ji} represents the influence of subgrid scale filting on the behavior of the large scales captured represented by the mesh. The lack of an analytical formulation for the exact representation of this tensor limits the solution by numerical models. A well-established model is the Smagorinsky (1963) model that represents the effects of the subgrid scales on the behavior of large scales, based on the equilibrium hypothesis for small ones. The Smagorinsky model describe that the turbulent viscosity subgrid is proportional to the velocity scale and to the length of the grid filter given by:

$$\upsilon_T = (C_s l)^2 \sqrt{\varepsilon_{ij} \varepsilon_{ij}}, \tag{16}$$

where C_s is the Smagorinsky constant.

The value of this parameter is a very sensitive issue because it is associated with the type of flow involved. In 1967, DK Lilly (*apud* Silveira Neto, 1998) determined the theoretical value $C_s = 0.18$, assuming isotropic and homogeneous turbulence. However, this value leads to excessive damping in fluctuations of large scales in shear flows or with solid boundaries, and in practice is reduced to approximately $C_s = 0.1$. Thus, C_s is not a universal constant, and may take values 0.065 at 2.0 (Ferziger & Peric, 2002).

The EdgeCFD software is a general-purpose finite element CFD software. It employs the SUPS formulation plus LSIC stabilization for the incompressible Navier-Stokes equations and the SUPG formulation with discontinuity- capturing for scalar transport (Elias & Coutinho, 2007), (Elias *et al*., 2008) and (Lins *et al*., 2009). EdgeCFD uses to treat turbulence by a Smagorinsky model (Elias & Coutinho, 2007).

This code uses a time integration predictor-multicorrector algorithm with adaptive time stepping by a Proportional-Integral-Derivative (PID) controller. Within the flow solution loop, the multi-correction steps correspond to the Inexact-Newton Krylov method. In this approach, the nonlinear solver adapts the tolerance according to the evolution of the solution residuum. EdgeCFD iterative driver is the Generalized Minimal Residual Method (GMRES) since the equation systems stemming from the incompressible flow and transport are non-symmetric. A nodal-block diagonal preconditioner is employed for the flow and a simple diagonal preconditioner for the transport equations. Most of the computational effort spent in the solution phase is devoted to matrix-vector products. To compute such operations more efficiently, we have used an edge-based data structure. The computations are performed in parallel using a distributed memory paradigm through the message passing interface library (MPI), using point-to-point communication. The parallel partitions are generated by the Metis library (Karypis & Kumar, 1998) while the information regarding the edges of the computational grid is obtained from the EdgePack library. EdgePack also reorders nodes, edges, and elements to improve data locality, exploiting the memory hierarchy of current processors efficiently. Integrals in EdgeCFD are computed using closed form relations derived in volume coordinates or using a one-point (centroid) integration rule. Thus, all coefficients in the element matrices and residue are explicitly coded.

3 EXAMPLE AND NUMERICAL MODEL

The example of flow past a fixed tapered circular cylinder presented in this paper is the model studied by Narasimhamurthy *et al.* (2009) for a Reynolds number range of 102 at the top and 300 at the base.

The geometric characteristics of the 3D computational domain used for the model are depicted in Fig. 5 and the specific values are shown in Table 1.

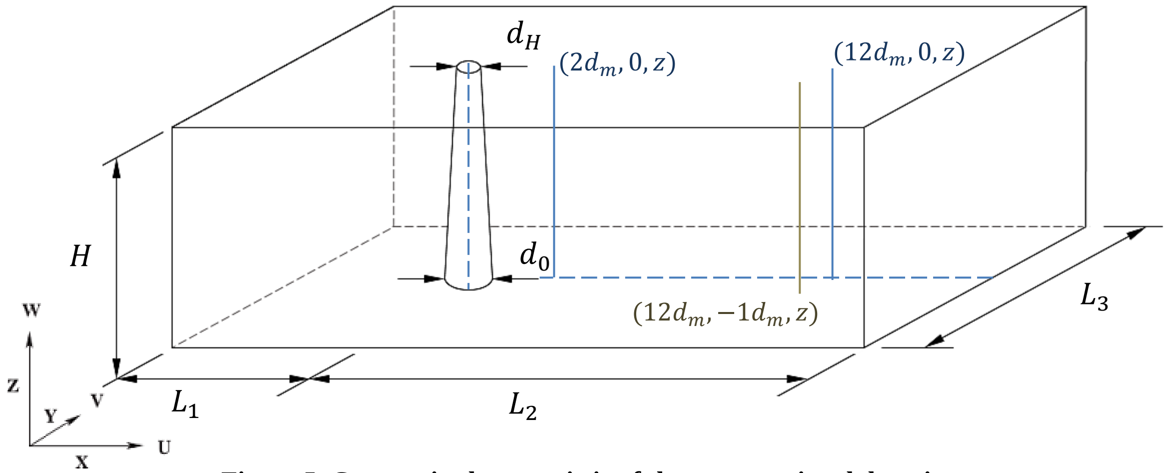

Figure 5. Geometric characteristic of the computational domain

Table 1. Details of the geometric characteristic of the computational domain (in cm)

Model	d_0	d_H	H	L_1	L_2	L_3
Narasimhamurthy *et al.* (2009)	1.0	0.34	49.5	6.5	15.5	13.0

A fine grid in the regions around and behind the cylinder is very important to the simulation, since in these regions occur the separation, backflow and vortex shedding phenomena. Therefore, it is used a grid refinement criterion in which regions approaching the cylinder are progressively more refined as shown in Fig. 6.

Proceedings of the XXXVIII Iberian Latin-American Congress on Computational Methods in Engineering
P.O. Faria, R.H. Lopez, L.F.F. Miguel, W.J.S. Gomes, M. Noronha (Editores), ABMEC, Florianópolis, SC, Brazil, November 5-8, 2017.

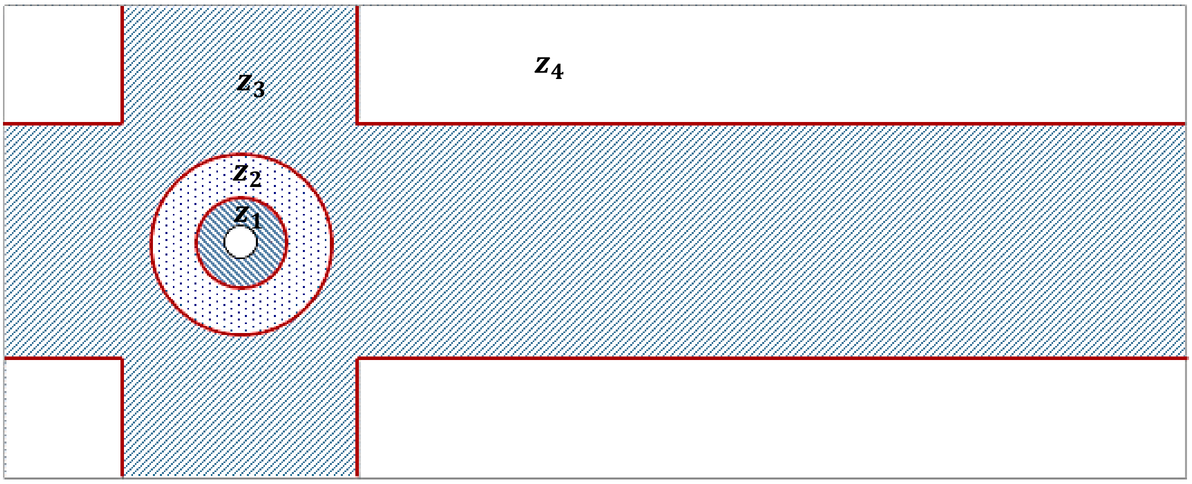

Figure 6. Regions of different discretization of the mesh. $z_1$is more refined zone and z_4 is less refined zone

For this model, it was employed a mesh with 8,600,063 elements, 1,448,143 nodes generated by Gmsh[1]. Figure 7 shows part of a vertical section ($12.375d_2 < z < 24.75d_2$) of the mesh passing through the cylinder axis, illustrating the different zones of discretization.

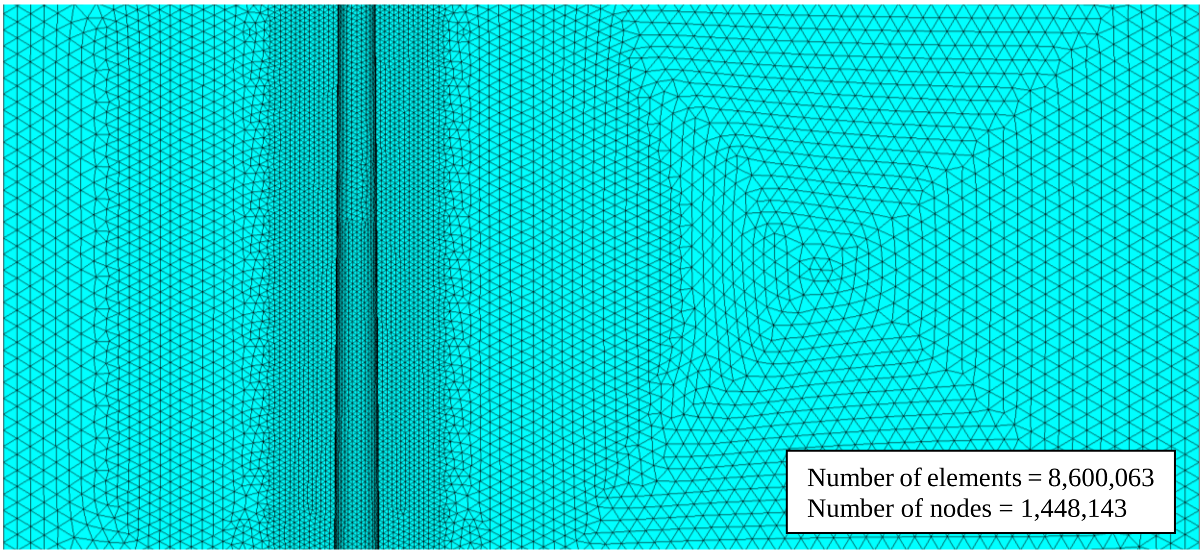

Figure 7. Regions of different discretization of the mesh, in the cylinder axis section between heights $12.375d_2$-$24.75d_2$.

To represent the boundary conditions used by the authors (Narasimhamurthy *et al.*, 2009), a free slip wall condition is applied to the top and bottom walls as well as on both side walls. A zero-static pressure condition is imposed on the outlet boundary and uniform velocity profile $U_o(= 1)$ was prescribed on the inlet boundary.

[1] http://geuz.org/gmsh/

4 RESULTS AND DISCUSSION

The results of the simulation are firstly presented in terms of time histories of the cross flow velocity V along two downstream lines parallel to the cylinder axis in Fig.8. These two lines are located (see Fig.5) at coordinates ($x = 2d_m$) and ($x = 12\ d_m$) being d_m the mean diameter of the cylinder.

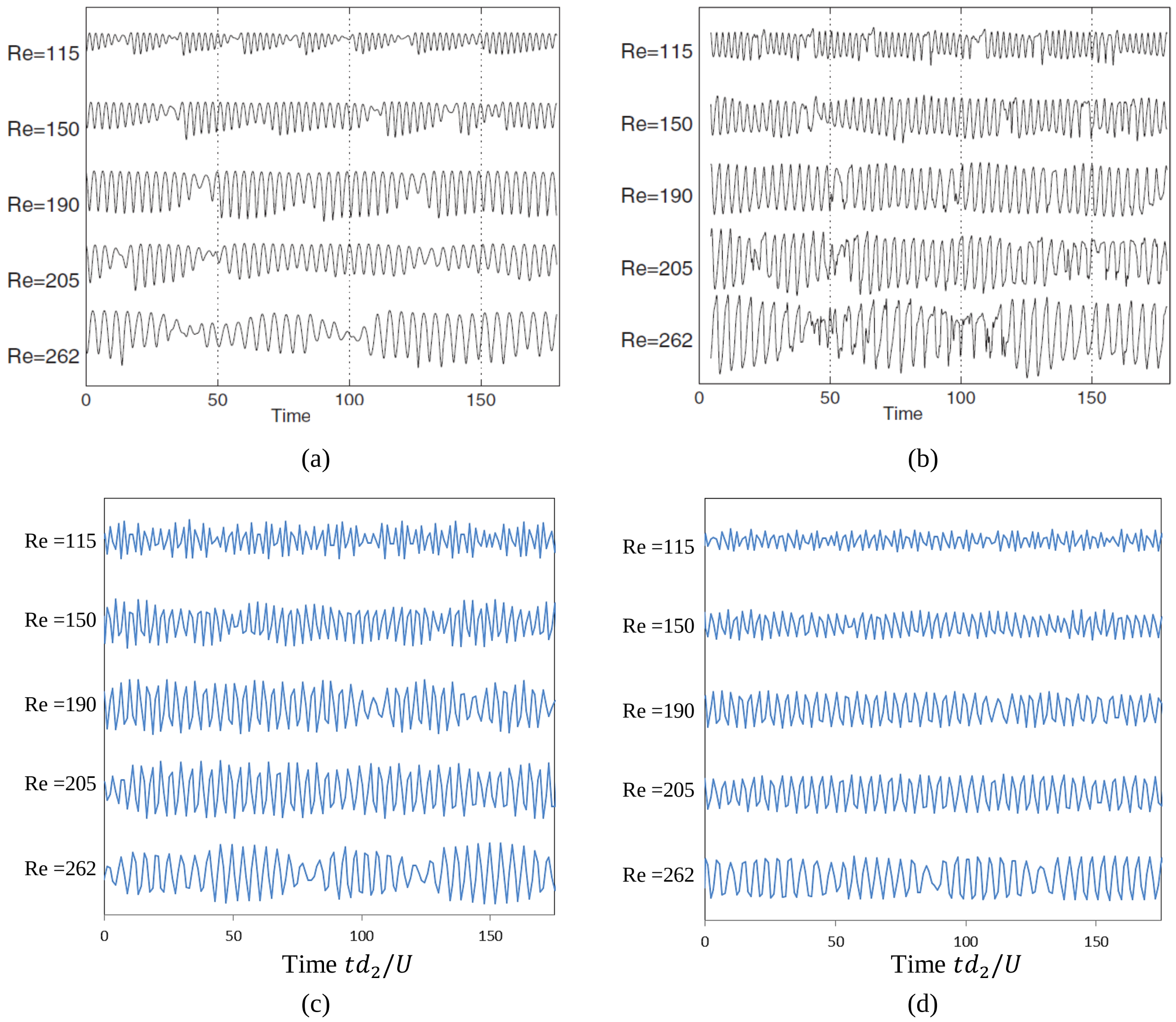

Figure 8. Times cross-flow velocity by local Reynolds number: (a) from $2d_m$ downstream (Narasimhamurthy *et al.* 2009); (b) from $12d_m$ downstream (Narasimhamurthy *et al.* 2009); (c) from $2d_m$ downstream (present study); (d) from $12d_m$ downstream (present study).

For the sake of comparison, Figs. 8a,b present the velocity V traces obtained by Narasimhamurthy *et al.* (2009) and Figs. 8c,d show the corresponding results obtained from the present simulation. The total sampling time covers about 36 vortex shedding cycles at the base and 65 cycles at the top. Overall similarity can be clearly seen between the compared results. Along the spanwise direction, Re varies from 102 (at the top) to 300 (at the base). Flows passing uniform cylinders are characterized as laminar for Re lower than 190 and as transitional for Re in the range 190 – 1000 (Williamson, 1996), with the appearance of fine-scale vortex modes and vortex dislocations. However, for tapered cylinders these three-dimensional features are present also for Re lower than 190. It can be noted in these figures that the velocity amplitudes are lower at the top than at the base. On the other hand, vortex frequencies are increased form the base to the top. Also noticeable is the presence of low-frequency modulations caused by vortex dislocations.

Figure 9 show frequency spectra of velocity V obtained by applying the Fast Fourier Transform to the corresponding time histories along the cylinder axis, both from Narasimhamurthy *et al.* (2009) results (Fig.9a) and the present simulation (Fig.9b). The spectra are superposed along the cylinder axis represented by Re_{local} ($= Ud_{local}/\nu$, d_{local} is the local diameter. The similarity between the results is clear despite the different perspectives of the figures. It is noted that the vortex frequency varies along the cylinder axis and that there are some regions of constant frequency, the so called vortex cells. This cellular pattern may be more clearly observed in Fig. 10a where the Strouhal number ($St = fd_m/U$) obtained by the present work is plotted against Re_{local} and compared to results from other authors showing good correlation. The step variations of St along the cylinder axis characterize the vortex cells while narrower regions in between may be seen as transition regions.

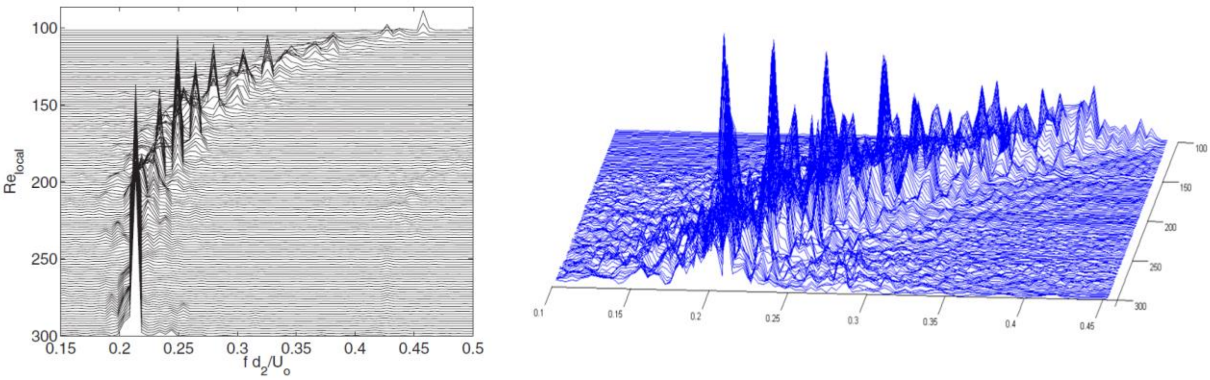

(a) (b)

Figure 9. Vortex shedding frequency from FFT by time velocity from $12d_m$ downstream: (a) Narasimhamurthy *et al.* (2009); (b) present study.

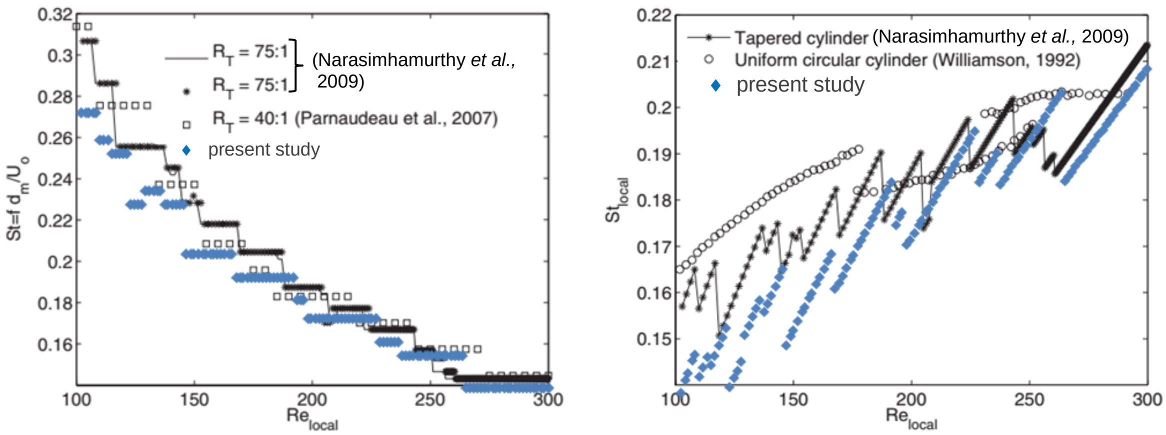

(a) (b)

Figure 10. Strouhal number *versus* local Reynolds number: (a) at d_m; (b) at d_{local}.

In Fig. 10b the local Strouhal number ($St = fd_{local}/U$) versus Re_{local} is presented. The curve related to the uniform cylinder shows continuous variation of St for increasing Re until the value of 190 is reached. At this point a discontinuity is observed which corresponds to the transition from the laminar mode to vortex loop mode (A) introducing three dimensional features to the flow (Williamson, 1996). Another discontinuity is present for Re equal to 260 corresponding to the transition to streamwise vortex pairs mode (B). For the tapered cylinder multiple discontinuities are observed all along the span related to vortex cells and adjacent regions.

Figure 11 illustrates with contour lines the cross-flow velocity along the cylinder axis at point with coordinates ($x = 12\ d_m$, $y = -1\ d_m$), for time instants in the range 80 to 180, displaying 21 vortex cycles at the base and 40 cycles at the top of the cylinder. Near the base the red colours and yellow at the top indicate peak values and the lines formed may be viewed as the vortex path. A vertical pattern denotes a region with the same vortex frequency and a kink in the vortex lines as marked by a circle in the figure indicates a vortex dislocation. Fig. 12 (Techet *et al.*, 1998) explains the behavior by illustrating each vertical vortex line at the base splitting in two lines and the intermediate oblique path towards the top where vertical lines are established.

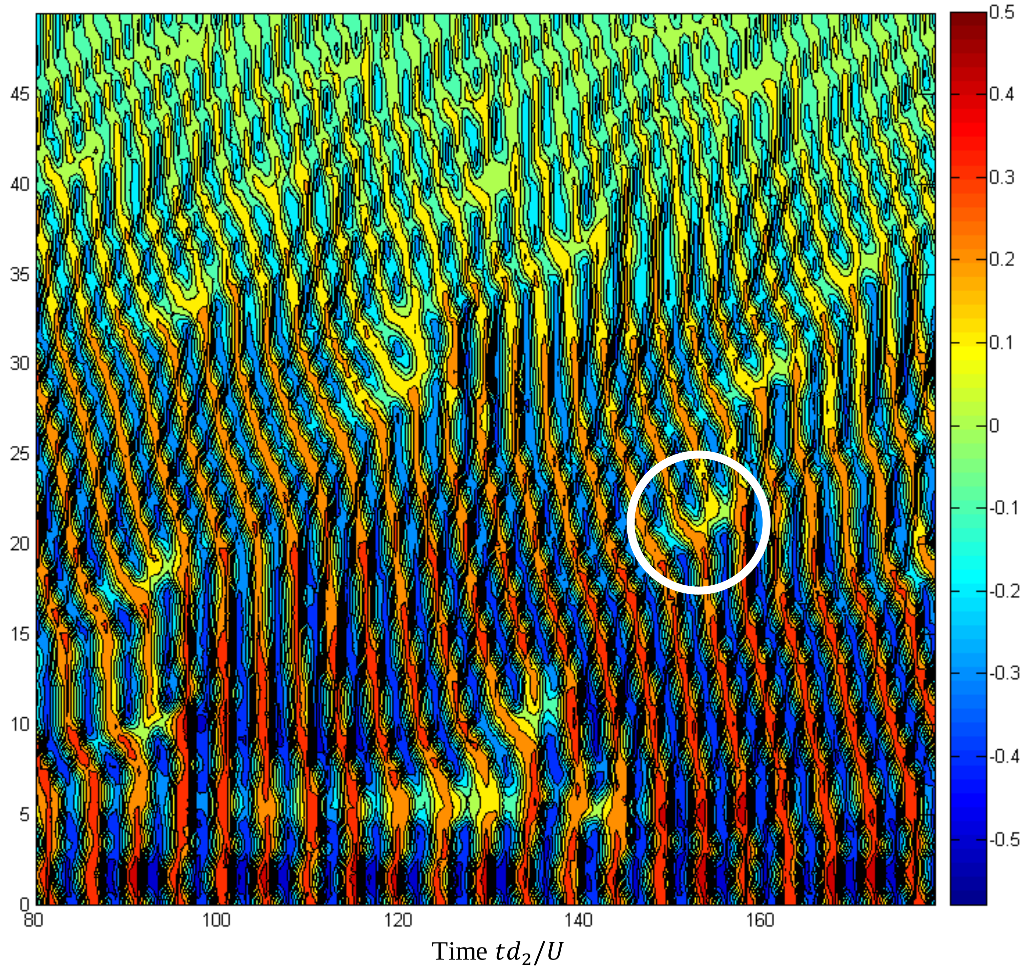

Figure 11. Pseudo-flow visualization of the cross-flow velocity at line located at coordinates ($x = 12\ d_m$, $y = -1\ d_m$).

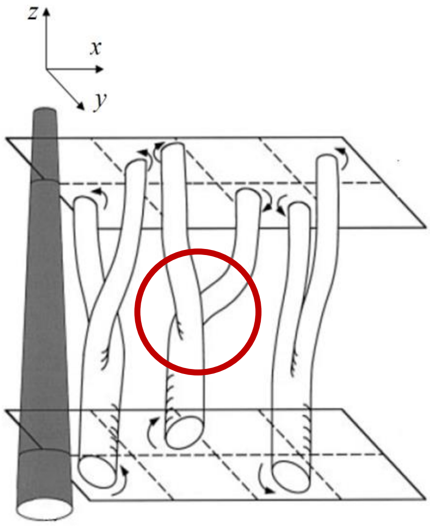

Figure 12. A sketch of the proposed 'hybrid' shedding mode (adapted Techet et al., 1998)

In Fig. 13 contour lines of the along-flow velocity at the same line of Fig. 11 are shown. It can be observed that the velocity variations at the base are larger than at the top.

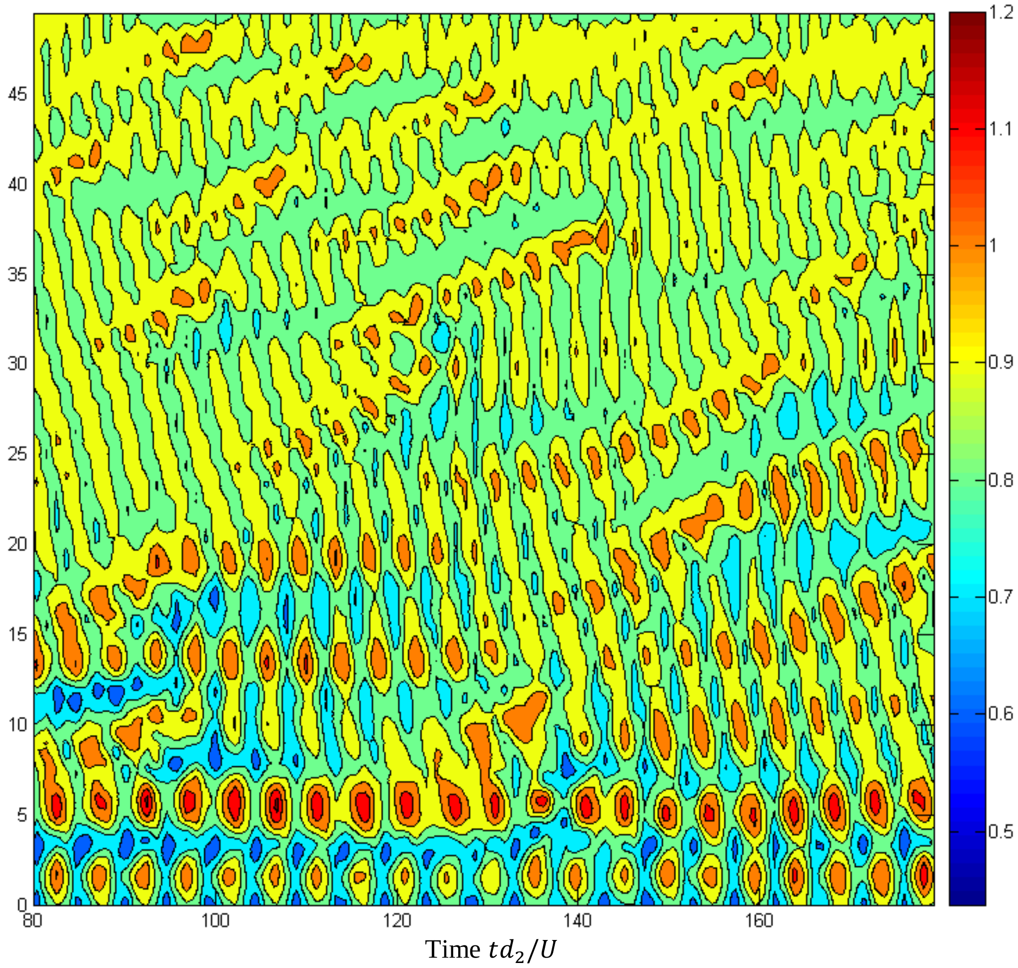

Figure 13. Pseudo-flow visualization for along-flow velocity at line located at coordinates ($x = 12\ d_m$, $y = -1\ d_m$).

The contour lines of the velocity in the spanwise (vertical) direction are illustrated in Fig. 14 where it can be noted that a secondary flow takes place as also observed by Narasimhamurthy et al. (2009).

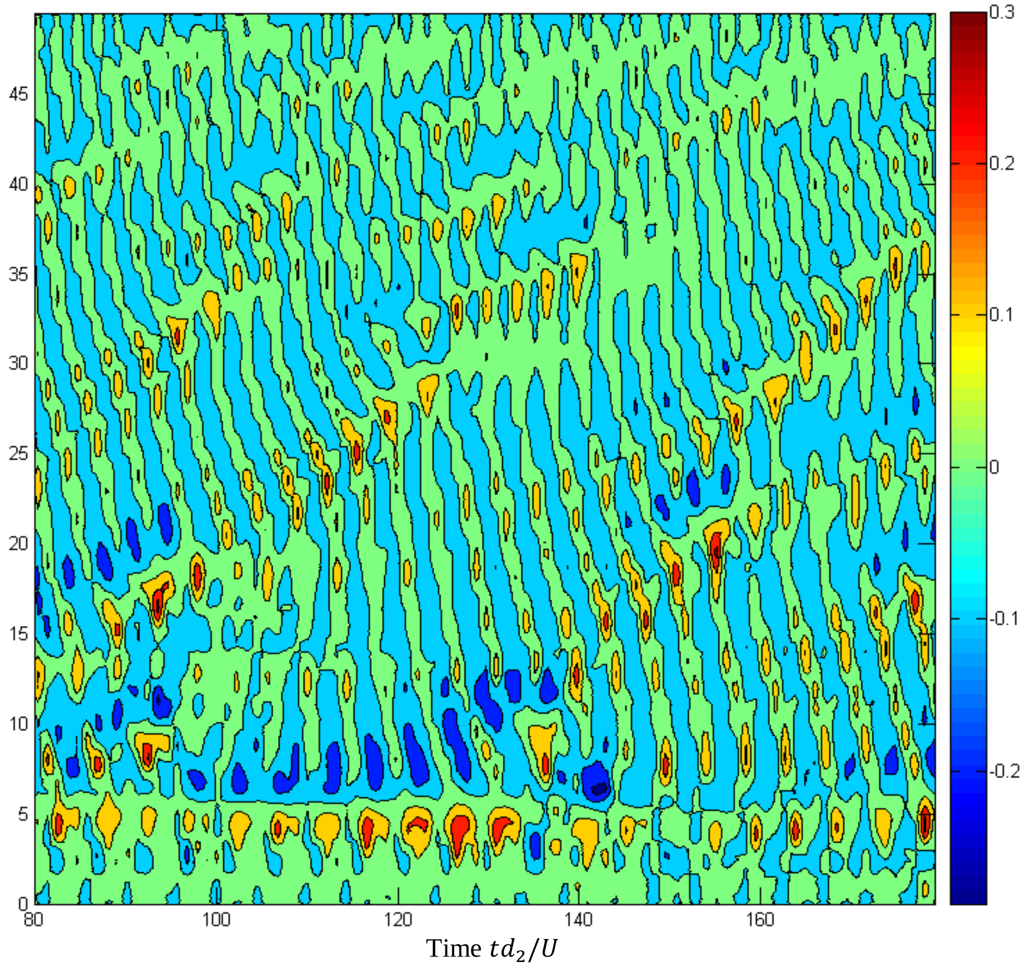

Figure 14. Pseudo-flow visualization for vertical velocity at line located at coordinates ($x = 12\ d_m$, $y = -1\ d_m$).

Figure 15 confirm the previous observations, illustrating the three-dimensional flow effect. At the top, the flow presents a large number of cycles of vortex shedding while at the base when number of cycles of vortex shedding is smaller. The eddies can be clearly identified in Fig. 15c by the change in the across-flow velocity.

Proceedings of the XXXVIII Iberian Latin-American Congress on Computational Methods in Engineering
P.O. Faria, R.H. Lopez, L.F.F. Miguel, W.J.S. Gomes, M. Noronha (Editores), ABMEC, Florianópolis, SC, Brazil, November 5-8, 2017.

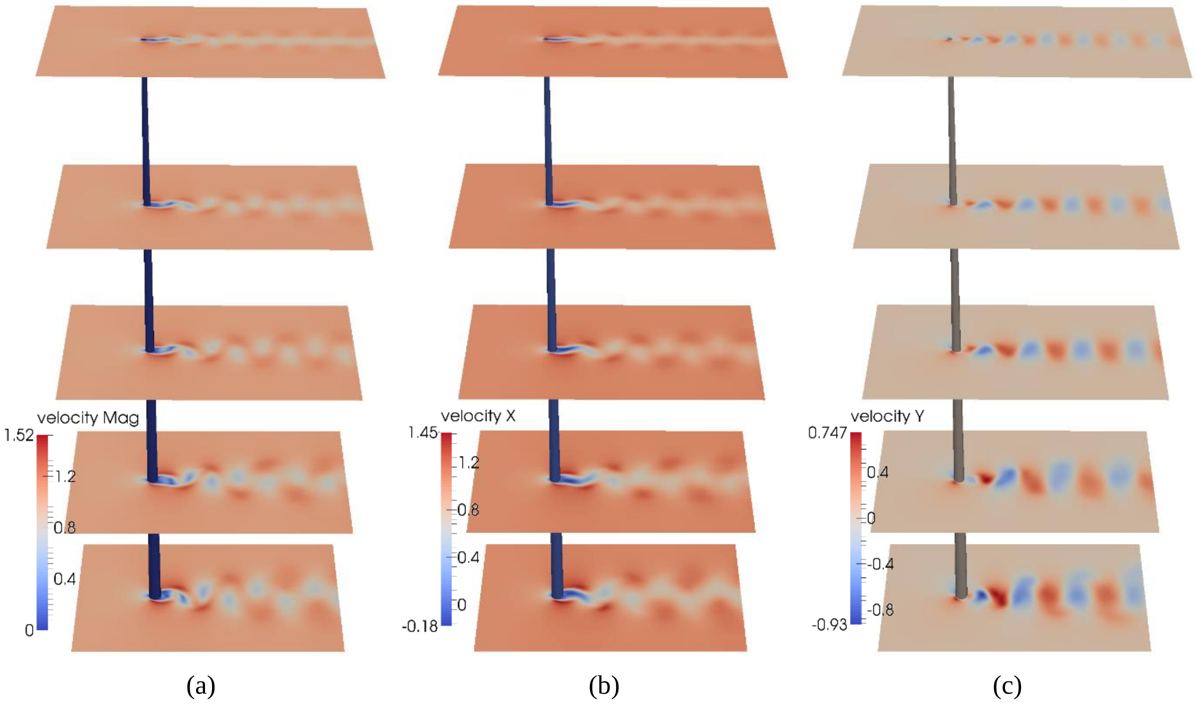

Figure 15. Flow velocity in different heights, at time $100d_2/U_0$: (a) resultant velocity; (b) along-flow velocity; (c) across-flow velocity.

Figures 16 present time histories of the resultant drag and lateral forces acting on the cylinder expressed as drag and lift coefficients referred to the mean diameter (C_D and C_L respectively). Mean values calculated in the range of time instant 30 to 180 are 1.1 for C_D (in good agreement with uniform long cylinders) and 0.0 for C_L (as expected). For this case peak values of the lateral force reach 15% of the nearly constant drag force. But peak lateral force may be greater than the drag force even for stationary (or *quasi*) cylinders, depending on many factors.

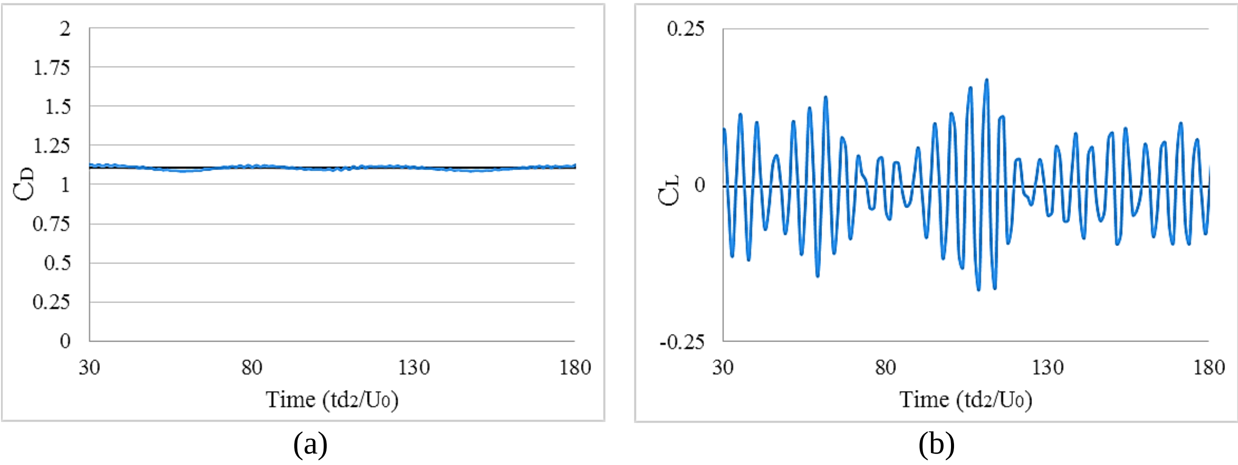

Figure 16. Time histories of the resultant forces coefficients in tapered cylinder (a) drag coefficient (C_D); (b) lift coefficient (C_L).

5 CONCLUSIONS

The present LES simulation focus on the study of the flow around a stationary tapered cylinder. Comparative analysis showed that results of the present study are similar to those obtained by Narasimhamurthy et al. (2009).

Contour lines of cross-flow velocity time histories, their corresponding spectra and the Strouhal number analysis confirmed the existence of vortex shedding cells of constant frequency along the height and also the occurrence of vortex dislocations or vortex splits.

The observed cellular pattern of the wake is also present at higher Reynolds numbers, typical of flows past chimneys and towers structures under wind loading, and has inspired one of the semi-empirical methods used to design these structures today: the Ruscheweigh method (Dyrbye & Hansen, 1997). However, questions are yet being raised in the literature on the adequacy of the models adopted in design codes to take into account the effect of the income wind turbulence on vortex-induced vibrations. Motivated by these questions new simulations are underway involving tapered cylinders under smooth and turbulent shear flow, at higher Reynolds numbers.

ACKNOWLEDGEMENTS

The research work reported in this paper was supported by MCTI/CNPq and MEC/CAPES, Brazilian agencies for scientific and technological development. Computer time at Lobo Carneiro supercomputer is provided by the High Performance Computer Center at COPPE/UFRJ, project a16010.

REFERENCES

Bargi, K., Tamimi, V. & Zeinoddini, M., 2015. VIV of Tapered Cylinders: 3D LES Numerical Simulation, *International Journal of Maritime Technology*, vol. 3, pp.: 17-31.

Blevins, R. D., 1977. *Flow Induced Vibration*. Van Nostrand Reinhold Company New York.

Dyrbye, C. & Hansen, S. O., 1997. *Wind Loads on Structures*, John Wiley & Sons.

Elias, R. N. & Coutinho, A. L. G. A., 2007. Stabilized edge-based finite element simulation of free-surface flows. *Journal for Numerical Methods in Fluids* vol. 54, pp.: 965-993.

Elias, R. N., Paraizo, P. L. B. & Coutinho, A. L. G. A., 2008. Stabilized edge-based finite element computation of gravity currents in lock-exchange configurations. *Journal for Numerical Methods in Fluids*, v. 57, pp.: 1137-1152.

Ferziger, J.H. & Peric, M., 1997. *Computational Methods for Fluid Dynamics*. Springer.

Hsiao, F.B. & Chiang, C.H., 1998. Experimental study of cellular shedding vortices behind a tapered circular cylinder, *Experimental Thermal and Fluid Science*, vol. 17, pp.: 179-188.

Karypis, G. & Kumar, V., 1998. *Metis 4.0: unstructured graph partitioning and sparse matrix ordering system.* Technical report. Department of Computer Science, University of Minnesota, Minneapolis.

König, M., Eisenlohr, H. & Eckelmann, H., 1992. Visualisation of the spanwise cellular structure of the laminar wake of wall-bounded circular cylinders. *Physics of Fluids*, vol. 4, 869

Lins, E. F., Elias, R. N., Guerra, G. M., Rochinha, F. A. & Coutinho, A. L. G. A., 2009. Edge-based finite element implementation of the residual-based variational multiscale method. *International Journal for Numerical Methods in Fluids*, v.61, pp.1-22.

Narasimhamurthy, V. D., Andersson, H. I. & Pettersen, B., 2009. Cellular vortex shedding behind a tapered circular cylinder, *Physics of Fluids*, vol. 21, 044106.

Silveira Neto, A., 1998. Large Eddy Simulation of Flow (in portuguese). In Freire, A.P. S., Menut, P. P. M., & Su, J., eds, *I Escola de Primavera de Transição e Turbulência (EPTT-1)*, pp. 157-190. ABCM.

Techet, A. H., Hover, F. S. & Triantafyllou, M. S., 1998. Vortical patterns behind a tapered cylinder oscillating transversely to a uniform flow. *Journal of Fluid Mechanics*, vol. 363, pp. 79-96.

Williamson, C. H. K., 1989. Oblique and parallel modes of vortex shedding in the wake street wake of cylinders at low Reynolds numbers. *Journal of Fluid Mechanics*, vol. 206, pp. 579-627.

Williamson, C. H. K., 1992. The natural and forced formation of spot-like vortex dislocations in the transition of a wake. *Journal of Fluid Mechanics*, vol. 243, pp. 393-441.

Williamson, C. H. K., 1996. Vortex dynamics in the cylinder wake. *Annual Review of Fluid Mechanics*, vol. 28, pp. 477-539.